Laser Excitation of the Th-229 Nucleus

J. Tiedau,* M.V. Okhapkin,* K. Zhang,* J. Thielking, G. Zitzer, E. Peik†
Physikalisch-Technische Bundesanstalt, 38116 Braunschweig, Germany

F. Schaden,* T. Pronebner, I. Morawetz, L. Toscani De Col, F. Schneider,
A. Leitner, M. Pressler, G.A. Kazakov, K. Beeks, T. Sikorsky, T. Schumm‡
Vienna Center for Quantum Science and Technology, Atominstitut, TU Wien, 1020 Vienna, Austria.
(Dated: March 12, 2024)

The 8.4 eV nuclear isomer state in Th-229 is resonantly excited in Th-doped CaF_2 crystals using a tabletop tunable laser system. A resonance fluorescence signal is observed in two crystals with different Th-229 dopant concentrations, while it is absent in a control experiment using Th-232. The nuclear resonance for the Th^{4+} ions in Th:CaF_2 is measured at the wavelength 148.3821(5) nm, frequency 2020.409(7) THz, and the fluorescence lifetime in the crystal is 630(15) s, corresponding to an isomer half-life of 1740(50) s for a nucleus isolated in vacuum. These results pave the way towards Th-229 nuclear laser spectroscopy and realizing optical nuclear clocks.

The resonant excitation of elementary quantum systems with coherent electromagnetic radiation is at the heart of many experiments in physics, like spectroscopy of atoms and molecules, atomic clocks, quantum information processing, and others. Coherent laser excitation has many applications, especially when highly precise control of frequency or phase of quantum superposition states is required, but it has hardly been used in nuclear physics to date [1]. The difficulty in laser excitation of nuclei is understandable from the huge mismatch between typical nuclear excitation energies and available laser photon energies. Nuclear excitation has been demonstrated in laser-produced plasmas, where the interaction is mediated via electrons that are accelerated in an intense laser field, and interact with the nucleus in collisions or via bremsstrahlung in the X-ray regime [2]. Different nuclei have been resonantly excited with synchrotron radiation on transitions in the energy range of 6-60 keV with lifetimes in the ns to μs range [3]. A 12.4 keV resonance in Sc-45 with a lifetime of 0.47 s has recently been excited at the European X-ray free-electron laser [4].

The Th-229 nucleus is known for its unique low-energy isomeric state [5–7]. Its excitation energy of 8.4 eV places the nuclear transition in the vacuum-ultraviolet (VUV) spectral range and makes it accessible for experiments with tabletop laser systems and the tools of precision optical frequency metrology. A number of proposals have been put forward based on these exceptional properties (see [8, 9] for recent reviews), including the concept of a nuclear optical clock of very high accuracy [10, 11] and high sensitivity in tests of fundamental physics [12, 13]. Reflecting the inherent robustness of nuclear transitions to external fields and chemical environment, even a solid-state version of an optical clock has been proposed, based on Th-229 doped into a VUV-transparent crystal, with a bandgap that is larger than the isomer energy. [14, 15]. Placing the atoms in a solid-state crystal lattice confines them to a region that is much smaller than the excitation wavelength (Lamb–Dicke regime), which suppresses the effects of photon recoil and first-order Doppler shift on the nuclear transition [15].

Previous attempts to excite the low-energy transition of the Th-229 nucleus with a laser or other light source have not been successful. Part of the difficulty resulted from a large uncertainty in the transition wavelength, that was initially determined from differences of much larger gamma photon energies [5]. Another difficulty arises from the fact that Th-229 is radioactive, undergoing alpha-decay with a half-life of 7825(87) years [16]. Consequently, the detection of a weak nuclear resonance fluorescence signal from a sample of Th-229 is hampered by a strong background of radioluminescence and Cherenkov radiation from several stages of the Th-229 decay chain [17–19]. Three unsuccessful attempts on excitation of Th-229 resonance in solid samples have been reported, using undulator radiation at electron storage rings, with spectral photon fluxes up to 100 photons/(s Hz) [20–22]. Covering a wide wavelength range between 120 and 300 nm, none of these experiments detected a signal related to the nuclear transition.

Recently, more precise information on the Th-229 transition energy was provided by three different experiments: an energy measurement of the electron emitted after internal conversion decay [23], gamma-spectroscopy using a cryogenic microcalorimeter [24], and vacuum-ultraviolet spectroscopy of Th-229 produced via beta-decay of Ac-229 at the ISOLDE facility at CERN [25]. The latter study is of strong relevance for the experiment reported here, because it achieved the first observation of the Th-229 radiative decay in CaF_2. This has shown that a detection of the VUV nuclear fluorescence in this material is not prevented by competing conversion decay via electronic states within the bandgap of the crystal, related to color centers or impurities.

In this letter we report the first laser excitation of the Th-229 nuclear transition. We use Th:CaF_2 crystals grown at TU Wien [26] with up to $5 \times 10^{18}/\mathrm{cm}^3$ Th-229 concentration, and a VUV laser system developed at

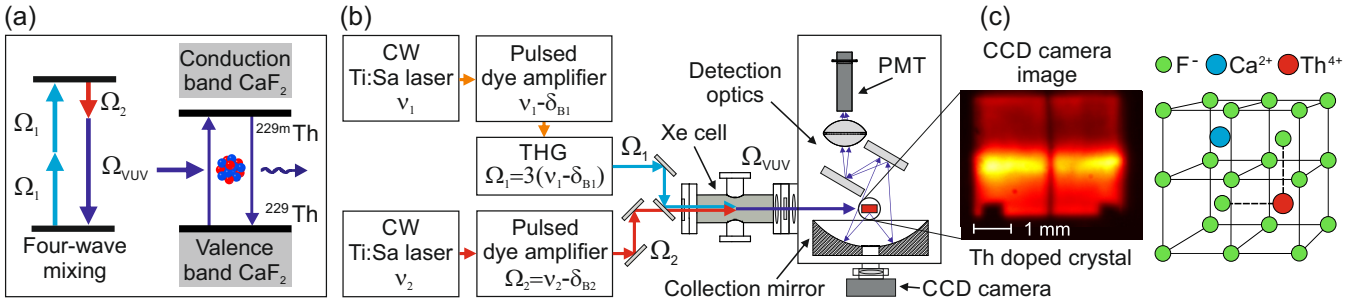

FIG. 1. Excitation scheme (a) and experimental apparatus (b) for VUV laser spectroscopy of the isomeric state in Th-doped crystals. The VUV source consists of two CW lasers with the frequencies ν_1, ν_2, two pulsed dye amplifiers that introduce frequency shifts $(\delta_{B1}, \delta_{B2})$ due to Brillouin mirrors, a THG stage and a xenon gas cell. The scanning is provided by tuning of the difference frequency Ω_2 via ν_2. The spectroscopy vacuum chamber contains the Th-doped crystal mounted on a cold finger, signal collection optics and a PMT. (c) False color CCD camera image of the crystal during VUV laser excitation and a schematic representation of the crystal structure of Th^{4+} ions doped into the CaF_2 lattice with $2F^-$ for interstitial charge compensation.

PTB, that provides a spectral photon flux of more than $2 \cdot 10^4$ photons/(s Hz) [27]. The experimental apparatus is shown schematically in Fig. 1.

Th-doped CaF_2 crystals were grown using the Vertical Gradient Freeze (VGF) method, a detailed description can be found in [26]. A modified VGF device was developed to achieve high doping concentrations with the scarcely available Th-229 isotope. To ensure chemical purity, synthetic CaF_2 was used as the starting material and PbF_2 as an oxygen scavenger [28]. The growth process took place at a high temperature of 1700 K, and a high vacuum of 10^{-4} Pa was maintained to prevent any potential contamination [29]. The resulting crystals were verified for chemical purity using optical and gamma spectroscopy. Radiolysis, occurring during growth using radioactive dopants, leads to a fluoride-deficiency of the resulting crystal, which drastically reduces the VUV transmission - up to full opaqueness in the case of crystal X2. We use annealing to the superionic phase of CaF_2 under 10^5 Pa of CF_4 gas to replenish the fluoride in the grown crystals, recovering VUV transmission and increasing radiation hardness [30]. Table 1 summarizes the key properties of the crystals used in this experiment.

TABLE I. Key parameters of Th-doped CaF_2 crystals.

Crystal Code	**X2**	**C10**	**V12**
Dopant isotope	Th-229	Th-229	Th-232
Th activity [kBq]	66	22	0
Concentration [cm^{-3}]	5×10^{18}	3×10^{17}	1×10^{19}
Column density [mm^{-2}]	8×10^{15}	1×10^{15}	4×10^{16}

The VUV source [27] consists of two CW Ti:sapphire (Ti:Sa) ring lasers with two pulsed dye amplification stages, a third harmonic generation (THG) unit, a Xe gas cell for the four-wave mixing and an ultra-high vacuum VUV beam line. It operates at a repetition rate of 30 Hz, with a pulse duration of 10 ns and mean pulse energy of $\approx 15\,\mu$J over the wavelength range 148.3 to 149.1 nm, the $\pm\sigma$-uncertainty range of the isomer transition according to [25]. The measured spectral linewidth of the VUV source is $\leq$10 GHz. This corresponds to a VUV power spectral density of $\approx$0.1 pW/Hz. The VUV beam is steered to the spectroscopy vacuum chamber using two high-reflective mirrors, each mounted on a motorized mirror holder. To ensure the correct beam alignment to the Th-doped crystal, two beam position quadrant detectors are used [27].

The spectroscopy vacuum chamber is separated from the VUV beam line by a MgF_2 vacuum viewport. The VUV beam diameter at this position is about 3 mm. The VUV radiation is further focused to a $\approx$0.5 mm diameter in the crystal by a MgF_2 lens. The Th-doped crystal is attached to a liquid nitrogen cooled finger that is mounted on a 3-axes vacuum manipulator. A low operating temperature ≤ 180 K is required to avoid optical damage of the Th-doped crystal under VUV exposure [31]. A spherical mirror is used to collect the crystal fluorescence over a large solid angle. The fluorescence is then directed to a Cs-I photomultiplier tube (PMT) by two dielectric mirrors. The mirrors are reflective over the wavelength range between 141 and 152 nm [34] and used to filter out the main part of the background of crystal radioluminescence [26]. A short focal length MgF_2 lens is used to focus the signal onto the PMT. To minimize direct exposure of the PMT with high-energy γ-radiation from the crystal, a lead shield is placed on the side of the crystal holder opposite to the collection mirror. A CCD camera and a laser pilot beam are used for imaging the crystal position and its overlap with the VUV radiation. The CCD camera also monitors the radioluminescence and photoluminescence of the crystals during VUV laser excitation and gives additional information about the transmission of the crystal.

The experimental sequence consists of alternating

VUV laser excitation and detection intervals. In the initial search of the isomer transition, we irradiate the crystal for $t_e = 120\,\mathrm{s}$ and record a PMT signal for $t_d = 150\,\mathrm{s}$. During the excitation cycle, the Ti:Sa laser frequency ν_2 (see Fig. 1) is scanned continuously with a triangular modulation of $\pm 15\,\mathrm{GHz}$ around the central value for each frequency step. The modulation speed is chosen such that the VUV pulses leave no gap in the scanned frequency. Meanwhile, the PMT is protected from scattered laser light by applying a $+300\,\mathrm{V}$ blocking voltage to the first dynode. During the detection time, the pump laser of the pulsed dye amplifiers is turned off to avoid VUV scattering light on the signal PMT, and the scanning laser frequency is moved to the next point.

The wavelength of the VUV source is determined by monitoring the frequencies (ν_1, ν_2) of the CW four-wave mixing lasers by a Fizeau wavemeter, taking into account a measured total frequency shift of $\Delta_B = -6\delta_{B1} + \delta_{B2} = -10.1(5)\,\mathrm{GHz}$ which appears in stimulated Brillouin scattering mirrors of the amplifiers [27]. To exclude possible systematic errors, we use two independent wavemeters, permanently calibrated with a clock laser of the Yb^+ optical frequency standard [32].

The background pressure in the spectroscopy vacuum chamber is about $10^{-5}\,\mathrm{Pa}$. During the operation of the VUV source we observe a buildup of polymeric carbon on the optical elements which are exposed to VUV radiation (see, for example, Ref. [33]). To remove surface carbon, hydrocarbons and organics from the optical viewport, the focusing lens and the crystal, we use an Evactron E50 de-contaminator for in situ plasma cleaning on a weekly basis.

An initial search for the isomer excitation covering the wavelength range from 148.2 nm to 150.3 nm was done using the C10 crystal (see table 1) with a lower concentration of ^{229}Th. The C10 crystal was used to prevent possible damage to the highly doped X2 crystal under the high pulse power of the VUV radiation over a long exposure time. The luminescence from the crystal produced a background PMT signal of 130 - 160 counts per second (cps) with a typical shot noise of $\leq \pm 2\,\mathrm{cps}$ when averaged over a 150 s detection cycle. The total search range was covered in approximately 20 measurement runs with ≈50 wavelength steps each [34]. The time per run is limited by the formation of an ice-layer on the cold crystal that absorbs VUV light. The ice-layer is detectable as a reduction of the VUV luminescence signal on the PMT with a time constant on the order of 5-6 hours. Therefore, a warm-up cycle for transmission recovery at room-temperature is applied after each run.

While scanning over the full range using the C10 crystal, we observe one clearly detectable fluorescence peak [34] at the excitation wavelength 148.38 nm. A scan around the same wavelength with the highly doped, freshly-fluorinated [30] X2 crystal shows an ≈25 times higher signal with the same frequency center position and similar shape as for C10 (Fig. 2(a)). The radioluminescence background of the X2 crystal is about 400 cps. The measured fluorescence signal and the estimated count rate [34, 35] are consistent within one order of magnitude. The signals are recorded with $\pm 5\,\mathrm{GHz}$ modulation of the VUV laser over the frequency steps, in order to exclude frequency gaps during the scanning. The width and the shape asymmetry of the observed resonances are determined by the VUV source linewidth and by the scanning rate, because the measurement time for one frequency step is shorter than the isomer lifetime (see Fig. 3). Reducing the scanning rate would lead to an additional distortion of the signal due to ice-layer formation. Figure 2(b) shows the shape of the resonances in the X2 crystal for both scanning directions (red-dashed and blue line) with a subtraction of the exponentially decaying contribution of the previous data points (see SM [34] for additional information). The full width of the resonances at half maximum is ≈20 GHz, which is in good agreement with the laser linewidth including the $\pm 5\,\mathrm{GHz}$ modulation. The line shapes for both scan directions show excellent agreement with one another.

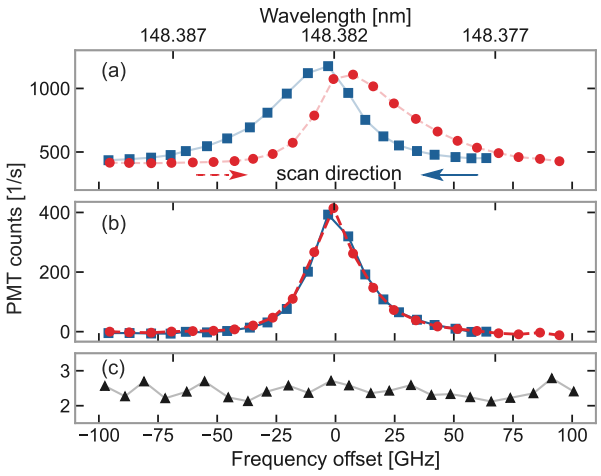

FIG. 2. (a) VUV fluorescence signals from the Th-229 doped X2 crystal, recorded in frequency scans from higher to lower frequency (squares) and lower to higher frequency (dots). The measurement time between frequency steps is shorter than the isomer decay time (see Fig. 3) which leads to an asymmetry in the resonance curves. (b) The resonance asymmetry is removed, together with the radioluminescence background, from the plots in (a) in post-processing. (c) Result of a control experiment with the Th-232 doped V12 crystal.

To confirm that the laser-induced VUV fluorescence signal is due to the excitation of the Th-229 isomeric state and not related to color centers or crystal defects, we perform a $\pm 1\,\mathrm{THz}$ scan around the transition frequency using the Th-232 doped crystal V12, with a thorium concentration exceeding the one of the X2 crystal and otherwise identical parameters for crystal growth (see table I) and laser excitation. No fluorescence signal above

the PMT dark noise level of 2.5(5) cps is observed (see Fig. 2(c)), confirming that the observed signal is isotope specific.

The peak positions of all of the scans performed with both crystals and different scan parameters, with and without frequency modulation [34], coincide within ±3 GHz uncertainty. The central frequency ν_0 of the nuclear transition calculated from the four-wave mixing $(6\nu_1 - \nu_2 + \Delta_B)$ is 2020.409(7) THz which corresponds to a wavelength of 148.3821(5) nm and an energy of 8.35574(3) eV. The given uncertainty accounts for statistical and systematic contributions. The resonance wavelength measured here is within the 1σ-uncertainty of the value reported in [25]. We do not observe any shifts of the resonance within the uncertainty of the measurement when varying the crystal temperature in the range between 110 K and 170 K.

Thorium atoms in a solid-state crystal lattice are confined in the Lamb–Dicke regime. Therefore, there is no sensitivity of the nuclear transition to recoil or first-order Doppler effects. The second-order Doppler effect leads to a shift and a broadening of the transition on the order of ≈100 Hz due to vibrations of the nuclei [14, 15]. The magnetic dipole interaction with randomly oriented spins of surrounding nuclei also contributes to a broadening of ≈200 Hz. The nuclear quadrupole splitting of the transition from gradients of the electric crystal field is estimated as $\lesssim$1 GHz [36]. The field shift of the nuclear transition frequency as a function of the number of electrons in the Th ion is expected to be $\lesssim$1 GHz [37]. To resolve the mentioned effects, a VUV source with a linewidth below 1 GHz is required.

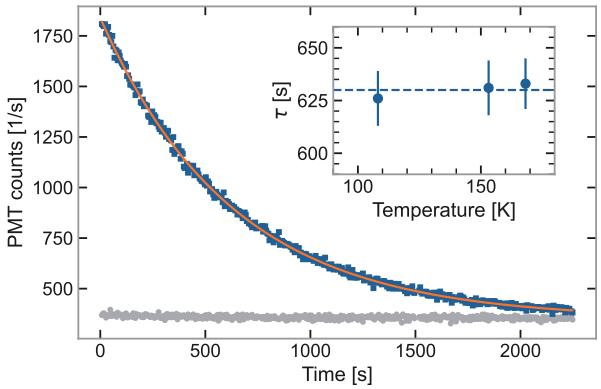

FIG. 3. Th-229 fluorescence decay curve after resonant excitation (blue trace) for 500 s measured with crystal X2 at a temperature of 150 K. Gray trace: result of a control experiment with 200 GHz off-resonant excitation, showing no long-lived photoluminescence. Inset: Fluorescence decay times for crystal temperatures between 108 K and 168 K. No changes in the decay time are observed within the measurement uncertainty. An overall decay time constant τ = 630(15) s is observed.

For the measurement of the fluorescence decay time constant, we stabilize the laser on the central position of the resonance and excite the isomeric state for 200-500 s. A typical signal obtained with the X2 crystal is shown in Fig. 3. The averaged decay time constant of the Th-229 isomeric state for the X2 crystal is 630(15) s. The signal decay observed using the C10 crystal is shown in [34], yielding a consistent value with larger uncertainty. Since the nuclei are present in the Th^{4+} charge state [36], we do not expect a significant contribution of bound internal conversion to the decay rate. A collective effect of radiation trapping is not expected because of the inhomogeneous spectral broadening, corresponding to about 10^6 natural linewidths.

The inset of Fig. 3 shows the results of measurements of the decay time for different temperatures of the crystal. Within the uncertainty, no influence of the temperature on the decay time is observed. For electronic transitions of rare-earth ions in crystals, temperature dependence of the radiative lifetime can be used to distinguish transitions that are phonon-assisted (coupling to the crystal field) from others that are not [38]. Also, luminescence effects that depend on a diffusion or transfer process would show a temperature-dependent rate, often in combination with a non-exponential time dependence [18]. The absence of a temperature dependence of the fluorescence lifetime observed in Th:CaF_2 and the purely exponential decay curve correspond to the expectations for a nuclear transition.

Because of the higher density of photon states in the dielectric optical medium, the spontaneous M1 decay rate is expected to be enhanced relative to the rate in vacuum by a factor n^3 where n is the refractive index [39]; $n \approx 1.586$ for CaF_2 at 148.4 nm [40, 41]. Applying this correction, the measured radiative lifetime of 630(15) s corresponds to an isomer half-life in vacuum of 1740(50) s, or a transition rate of $B(M1) = 0.022$ in Weisskopf units (W.u.). Different theoretical works had predicted transition rates in the range 0.006 to 0.05 W.u. (see discussions in [42, 43]). Two measurements of the Th-229 isomer half-life with larger uncertainty have been reported recently, based on population of the isomer in radioactive decay: $T_{1/2}$ = 2210(340) s measured for Th:MgF_2 ($n = 1.488$) [25] and $T_{1/2} = 1400^{+600}_{-300}$ s for trapped Th^{3+} ions [44]. All three results are in fair agreement.

In conclusion we have demonstrated the first laser excitation of the Th-229 low-energy nuclear transition, have reduced the uncertainty in the transition frequency by nearly three orders of magnitude, and have performed a precision measurement of the isomer lifetime. This opens the way towards nuclear laser spectroscopy of Th-229 in different host crystals and with trapped ions in different charge states, including the study of phenomena like electronic bridge processes [6, 7, 45], collective effects in nuclear scattering [46], and optical nuclear clocks with applications in tests of fundamental physics [13].

The development of dedicated VUV lasers with narrow linewidth will make it possible to access a new regime of resolution and accuracy in laser Mössbauer spectroscopy and to perform coherent control of a nuclear excitation [13].

Acknowledgements.–We would like to thank T. Leder and M. Menzel for the design and manufacture of the mechanical structures, N. Huntemann for providing an Yb-clock frequency reference for the wavelength measurements, N. Hosseini, J. Sterba, V. Rosecker, D. Hainz and M. Veit-Öller for support in the preparation, characterization, and handling of radioactive samples, S. Takatori, T. Hiraki, K. Yoshimura for support in early phases of the experiment preparation. This work has been funded by the European Research Council (ERC) under the European Union's Horizon 2020 research and innovation programme (Grant Agreement No. 856415), the Deutsche Forschungsgemeinschaft (DFG) – SFB 1227 - Project-ID 274200144 (Project B04), and by the Max-Planck-RIKEN-PTB-Center for Time, Constants and Fundamental Symmetries. The research was further supported by the Austrian Science Fund (FWF) Projects: I5971 (REThorIC), F1004 (Comb.at), and P33627 (NQRclock). Furthermore K. Beeks acknowledges support from the Schweizerischer Nationalfonds (SNF), fund 514788 "Wavefunction engineering for controlled nuclear decays". We thank the National Isotope Development Center of DoE and Oak Ridge National Labs for providing the Th-229 used in this work.

* These authors contributed equally to this work.
† email: ekkehard.peik@ptb.de
‡ email: thorsten.schumm@tuwien.ac.at

[1] T.J. Bürvenich, J. Evers, C.H. Keitel. Phys. Rev. Lett. **96**, 142501 (2006).
[2] K.W.D. Ledingham, P. McKenna, R.P. Singhal. Science **300**, 1107 (2003).
[3] E.E. Alp, W. Sturhahn, T.S. Toellner, J. Zhao, B.M. Leu, In: Kalvius, M., Kienle, P. (eds) The Rudolf Mössbauer Story. Springer, Berlin, Heidelberg, 339-356 (2012).
[4] Y. Shvyd'ko, R. Röhlsberger, O. Kocharovskaya, J. Evers, G.A. Geloni, P. Liu, D. Shu, A. Miceli, B. Stone, W. Hippler, B. Marx-Glowna, I. Uschmann, R. Loetzsch, O. Leupold, H.-C. Wille, I. Sergeev, M. Gerharz, X. Zhang, C. Grech, M. Guetg, V. Kocharyan, N. Kujala, S. Liu, W. Qin, A. Zozulya, J. Hallmann, U. Boesenberg, W. Jo, J. Möller, A. Rodriguez-Fernandez, M. Youssef, A. Madsen, T. Kolodziej, Nature **622**, 471 (2023).
[5] R.G. Helmer and C.W. Reich, Phys. Rev. C **49**, 1845 (1994).
[6] S. Matinyan, Physics Reports **298**, 199 (1998).
[7] E.V. Tkalya, Physics Uspekhi **46**, 315 (2003).
[8] P. G. Thirolf , B. Seiferle, L. von der Wense, J. Phys. B **52**, 203001 (2019).
[9] K. Beeks, T. Sikorsky, T. Schumm, J. Thielking, M.V. Okhapkin, E. Peik, Nature Rev. Phys. **3**, 238 (2021).
[10] E. Peik, C. Tamm, Europhys. Lett. **61**, 181 (2003).
[11] C.J. Campbell, A.G. Radnaev, A. Kuzmich, V.A. Dzuba, V.V. Flambaum, A. Derevianko, Phys. Rev. Lett. **108**, 120802 (2012).
[12] V.V. Flambaum, Phys. Rev. Lett. **97**, 092502 (2006).
[13] E. Peik, T. Schumm, M.S. Safronova, A. Pálffy, J. Weitenberg, P.G. Thirolf. Quantum Sci. Technol. **6**, 034002 (2021).
[14] W.G. Rellergert, D. DeMille, R.R. Greco, M.P. Hehlen, J.R. Torgerson, E.R. Hudson. Phys. Rev. Lett. **104**, 200802 (2010).
[15] G.A. Kazakov, A.N. Litvinov, V.I. Romanenko, L.P. Yatsenko, A.V. Romanenko, M. Schreitl, G. Winkler, T. Schumm. New J. Phys. **14**, 083019 (2012).
[16] R.M. Essex, J.L. Mann, R. Collé, L. Laureano-Perez, M.E. Bennett, H. Dion, R. Fitzgerald, A.M. Gaffney, A. Gourgiotis, A. Hubert, K.G.W. Inn, W.S. Kinman, S.P. Lamont, R. Steiner, R. W. Williams. J. Radioanal. Nucl. Chem. **318**, 515 (2018).
[17] E. Peik, K. Zimmermann, Phys. Rev. Lett. **111**, 018901 (2013).
[18] S. Stellmer, M. Schreitl, T. Schumm. Sci. Rep. **5**, 15580 (2015).
[19] S. Stellmer, M. Schreitl, G.A. Kazakov, J.H. Sterba, T. Schumm. Phys. Rev. C **94**, 014302 (2016).
[20] J. Jeet, C. Schneider, S.T. Sullivan, W.G. Rellergert, S. Mirzadeh, A. Cassanho, H.P. Jenssen, E.V. Tkalya, E.R. Hudson. Phys. Rev. Lett. **114**, 253001 (2015).
[21] A. Yamaguchi, M. Kolbe, H. Kaser, T. Reichel, A. Gottwald, E. Peik, New J. Phys. **17**, 053053 (2015).
[22] S. Stellmer, G. Kazakov, M. Schreitl, H. Kaser, M. Kolbe, T. Schumm, Phys. Rev. A **97**, 062506 (2018).
[23] B. Seiferle, L. von der Wense, V. Pavlo, I. Amersdorffer, C. Lemell, F. Libisch, S. Stellmer, T. Schumm, C.E. Düllmann, A. Pálffy, P.G. Thirolf, Nature **573**, 243 (2019).
[24] T. Sikorsky, J. Geist, D. Hengstler, S. Kempf, L. Gastaldo, C. Enss, C. Mokry, J. Runke, C.E. Düllmann, P. Wobrauschek, K. Beeks, V. Rosecker, J.H. Sterba, G. Kazakov, T. Schumm, A. Fleischmann, Phys. Rev. Lett. **125**, 142503 (2020).
[25] S. Kraemer, J. Moens, M. Athanasakis-Kaklamanakis, S. Bara, K. Beeks, P. Chhetri, K. Chrysalidis, A. Claessens, T.E. Cocolios, J.G.M. Correia, H. De Witte, R. Ferrer, S. Geldhof, R. Heinke, N. Hosseini, M. Huyse, U. Köster, Y. Kudryavtsev, M. Laatiaoui, R. Lica, G. Magchiels, V. Manea, C. Merckling, L.M.C. Pereira, S. Raeder, T. Schumm, S. Sels, P.G. Thirolf, S. Malven Tunhuma, P. Van Den Bergh, P. Van Duppen, A. Vantomme, M. Verlinde, R. Villarreal, U. Wahl, Nature **617**, 706 (2023).
[26] K. Beeks, T. Sikorsky, V. Rosecker, M. Pressler, F. Schaden, D. Werban, N. Hosseini, L. Rudischer, F. Schneider, P. Berwian, J. Friedrich, D. Hainz, J. Welch, J.H. Sterba, G. Kazakov, T. Schumm, Scientific Reports **13**, 3897 (2023).
[27] J. Thielking, K. Zhang, J. Tiedau, J. Zander, G. Zitzer, M.V. Okhapkin, E. Peik, New J. Phys. **25**, 083026 (2023).
[28] I. Nicoara, M. Paraschiva, M. Stef, F. Stef, Eur. Phys. J. B **85**, 292 (2012).
[29] T. Yonezawa, J. Nakayama, K. Tsukuma, Y. Kawamoto, Journal Of Crystal Growth **244**, 63 (2002)
[30] K. Beeks, T. Sikorsky, F. Schaden, M. Pressler, F. Schneider, B.N.Koch, T. Pronebner, D. Werban, N. Hosseini, G. Kazakov, J. Welch, J.H. Sterba, F. Kraus, T. Schumm,

arXiv:2312.13713v1 (2023)
[31] K. Beeks, Ph.D. thesis, TU Wien, (2022).
[32] R. Lange, N. Huntemann, J.M. Rahm, C. Sanner, H. Shao, B. Lipphardt, C. Tamm, S. Weyers, E. Peik. Phys. Rev. Lett. **126**, 011102 (2021).
[33] I. Yao-Leclerc, S. Brochet, C. Chauvet, N. De Oliveira, J.-P. Duval, J.-F. Gil, S. Kubsky, B. Lagarde, L. Nahon, F. Nicolas, M. Silly, F. Sirotti, M. Thomasset, Proc. SPIE **8077** 244 (2011).
[34] See Supplemental Material at http://link.aps.org/ supplemental...., which includes Refs. [22,26,28,30].
[35] R.C. Hilborn, Am. J. Phys. **50**, 982 (1982).
[36] P. Dessovic, P. Mohn, R.A. Jackson, G. Winkler, M. Schreitl, G. Kazakov, T. Schumm, J. Phys.: Condens. Matter **26**, 105402 (2014).
[37] V.A. Dzuba, V.V. Flambaum, Phys. Rev. Lett. **131**, 263002 (2023).
[38] M.J. Weber, Phys. Rev. **171**, 283 (1968).
[39] G. Nienhuis, C. Th. J. Alkemade, Physica (Amsterdam) **81**, 181 (1976).
[40] Q. Zheng, X. Wang, D. Thompson, Optical Materials Express **13**, 2380 (2023).
[41] M. Daimon, A. Masumura. Appl. Optics **41**, 5275 (2002).
[42] E.V. Tkalya, C. Schneider, J. Jeet, E.R. Hudson, Phys. Rev. C **92**, 054324 (2015).
[43] N. Minkov, A. Pálffy, Phys. Rev. Lett. **118**, 212501 (2017).
[44] A. Yamaguchi, Y. Shigekawa, H. Haba, M. Wada, H. Katori, presented at the 9th Symposium on Frequency Standards and Metrology, Kingscliff, NSW, Australia, 16-20 October 2023. (unpublished).
[45] B. S. Nickerson, M. Pimon, P. V. Bilous, J. Gugler, K. Beeks, T. Sikorsky, P. Mohn, T. Schumm, and A. Pálffy, Phys. Rev. Lett. **125**, 032501 (2020).
[46] B. S. Nickerson, W.-T. Liao, and A. Pálffy, Phys. Rev. A **98**, 062520 (2018).